Microchemical Journal 224 (2026) 117793

Contents lists available at ScienceDirect

Microchemical Journal

journal homepage: www.elsevier.com/locate/microc

Design of molecularly imprinted nanogels-based electrochemical sensor for the early detection of a myocardial damage biomarker

Francesco Gagliani [a], Tiziano Di Giulio [a], Muhammad Ibrar Asif [a], Noel Angelo Kalacas [b], Claudia Herrera-León [b], Alessia Di Fiore [b], Serena Laschi [d], Francesco Ranaldi [c,d], Paola Faraoni [c,d], Gabriele Giancane [e], Cosimino Malitesta [a], Karsten Haupt [b,f,*], Elisabetta Mazzotta [a,*]

[a] Laboratory of Analytical Chemistry, Department of Biological and Environmental Sciences and Technologies, University of Salento, Via Monteroni, 73100 Lecce, Italy
[b] Université de Technologie de Compiègne, UMR CNRS 7025 Enzyme and Cell Engineering, Rue du Docteur Schweitzer, CS 60319, 60203 Compiègne, France
[c] Department of Experimental and Clinical Biomedical Sciences "Mario Serio", University of Florence, Viale Pieraccini 6, 50139 Florence, Italy
[d] "Nanobiosens" Joint Lab, University of Florence, 50139 Florence, Italy
[e] Department of Cultural Heritage, University of Salento, Via D. Birago 64, 73100 Lecce, Italy
[f] Institut Universitaire de France, Paris, France

ARTICLE INFO

Keywords:
Molecularly imprinted nanogels
Molecularly imprinted nanoparticles
Impedimetric detection
Cardiac troponin T
Electrochemical sensor

ABSTRACT

Molecularly imprinted nanoparticles (MIP-NPs) are recognition elements obtained upon the polymerization of functional monomers around the target template, that, once removed, reveal selective binding sites in the polymeric matrix enabling the target binding with high specificity. Due to their small size, the binding sites are mostly located at the surface of the polymer, which definitely improves the binding kinetics. Solid-phase synthesis with an excess of the functional monomer NIPAm (N-isopropylacrylamide) confers a thermoresponsive character to the polymers, thus acquiring a solvated gel-like nanometer-sized feature, while the use of a protein epitope avoids the challenging issues related to the whole protein imprinting. Once produced, epitope-imprinted nanogels (MIP-NGs) can be anchored onto the surface of electrochemical transducers, thus leading to the development of selective electrochemical sensors.

In this work, MIP-NGs for the cardiac cell damage biomarker cardiac troponin T (cTnT) were anchored onto screen-printed carbon electrodes, enabling a linear impedimetric response in the concentration range 0.01–0.3 ng/mL with a LOD of 0.004 ng/mL. The sensor showed a negligible response towards interfering proteins and a reliable detection of the target protein in undiluted serum. To the best of our knowledge, for the first time an electrochemical sensor based on molecularly imprinted nanogels produced by solid-phase synthesis in aqueous environment with a protein epitope as template was developed for the detection of cTnT. The sensor featured analytical performances comparable to currently available immunoassays, thus showing a striking potential application as alternative tool for myocardial damage biomarker detection.

1. Introduction

Troponin T (TnT) is a protein member of the troponin complex, along with troponin C (TnC) and troponin I (TnI), constituting a regulation apparatus of skeletal and cardiac muscle contraction, where TnT is involved in the complex anchoring to the thin filament. While TnC is present in both skeletal and cardiac muscles, TnI and TnT are specific for cardiomyocytes, thus referred to as cardiac troponin I (cTnI) and cardiac troponin T (cTnT), respectively [1]. Being an internal component of myofibril contractile apparatus, cTnT blood levels are normally extremely low. Therefore, higher concentrations of the protein in the blood are indicative of a cardiac muscle damage as a result of pathological release from the myocardial cells [2], observed both in cardiac pathologies and non-cardiac/systemic causes, such as renal insufficiency

* Corresponding authors at: Université de Technologie de Compiègne, UMR CNRS 7025 Enzyme and Cell Engineering, Rue du Docteur Schweitzer, CS 60319, 60203 Compiègne, France (K. Haupt); Laboratory of Analytical Chemistry, Department of Biological and Environmental Sciences and Technologies, University of Salento, Via Monteroni, 73100 Lecce, Italy (E. Mazzotta).
E-mail addresses: karsten.haupt@utc.fr (K. Haupt), elisabetta.mazzotta@unisalento.it (E. Mazzotta).

https://doi.org/10.1016/j.microc.2026.117793
Received 20 November 2025; Received in revised form 3 March 2026; Accepted 19 March 2026
Available online 20 March 2026

or sepsis, or physiological conditions [3], with cut-off levels established in the concentration range 0.05–0.1 ng/mL [4]. Recent studies confirmed the blood circulation of cTnT in a time-dependent fashion: early presenting patients show high percentages of ternary complex and single protein, while late presentation is associated with the presence of smaller protein fragments [5]. Some studies highlight additional clinical relevance of cTnT due to its correlation with mortality in patients suffering from end-stage renal disease [6,7] or with pneumonia. Moreover, the higher cytoplasmic free cTnT concentration compared to cTnI (8% *vs.* 3%) quickens the cTnT blood circulation, thus highlighting its importance as myocardial injury biomarker [8].

The cTnT detection techniques are generally based on immunoassays, such as ECLIA, a chemiluminescence immunoassay involving the light emission from electro-generated species by using capturing antibodies [9,10]. Although cTnT sensitive assays with low detection limits (ng/mL) are available [11], several challenges should be considered, such as high-cost instrumentation, need of trained personnel and long operation times [12], along with the discrepancy among diagnostic kits, based on monoclonal antibodies for different protein epitopes [13–15], and a high interfering effect from heterophilic antibodies or hemoglobin due to a massive hemolysis leading to false negative results [16]. Therefore, it is essential to develop highly sensitive and specific detection systems for the rapid biomarker identification at the Point-Of-Care Testing (POCT) [17]. Electrochemical sensors offer a suitable alternative, due to their versatility, sensitivity, and rapid response. Their easy miniaturization/portability makes them ideal devices for POCT applications, enabled by the increasing use of low-volumes and low-cost printed electrodes [18]. Electrochemical detection strategies of cTnT are mostly based on antibodies and aptamers, which were reviewed in some recent papers [19,20]. Alternatively, molecularly imprinted polymers (MIPs) as biomimetic recognition elements gained much attention due to their stability, analyte binding capacity similar to that of bioreceptors and affordable production cost. MIPs are obtained upon the polymerization of functional monomers around a template, representing the analyte itself or a derivative, whose removal results in the formation of imprinted binding sites to which the analyte can specifically rebind, thus mimicking the biomolecular recognition phenomenon [21].

Recently, molecularly imprinted nanoparticles (MIP-NPs) showed to be highly performing recognition elements because of the high surface-to-volume ratio allowing the formation of imprinted binding sites mostly at the surface of the polymeric matrix, thus improving the binding kinetics of the analyte [22]. Their employment as recognition elements in electrochemical sensors clearly requires the integration with the transducer surface, which can be achieved by adopting different strategies, such as the entrapment in a polymeric matrix [23,24] and coupling chemistry mediated by SAM [25] or electrografted layers [26]. One of the disadvantages in MIP-NPs synthesis is represented by the often extreme conditions, such as high temperatures and organic solvents as polymerization media [27,28], possibly compromising the imprinting of biological molecules and environment and operator's safety. Therefore, the current trend is towards methods able to produce imprinted nanoparticles compatible with aqueous environments. Moreover, when proteins are to be used as templates, several challenges must be faced, such as size, structural complexity and flexibility and expensive production costs [29]. In this context, our group recently developed a solid-phase synthesis variant of MIP-NPs involving the template immobilization onto a solid support and a high molar fraction of N-isopropylacrylamide (NIPAm) in the monomer composition, conferring a thermoresponsive character to the polymer [30,31]. Considering the global monomer composition (mainly acrylamides) and the quasi-solubility of the low cross-linked (5 mol% bisacrylamide) polymer in the synthesis solvent water, the MIP nanoparticles are nanogels, completely solvated gel-like nanometer-sized particles (MIP-NGs). Accordingly, MIP-NGs undergo a volume-phase transition at the lower critical solution temperature (LCST, here ~32 °C), thus acquiring a compact, partly dehydrated structure at 37 °C, while being fully hydrated and swollen at 4 °C [32]. Due to this thermoresponsive behaviour, MIP-NGs can be synthesized at 37 °C in aqueous environment and eluted from the immobilized template at 4 °C [33,34]. The solid phase allows synthesis and purification steps to be performed directly *in situ*, without any further steps [32], while the oriented immobilization of the target template grants the formation of homogeneous binding sites and enables its re-use for at least another round of synthesis, thus reducing production costs and improving industrial manufacturing [33]. To overcome the challenging imprinting of proteins, a protein epitope can be employed as template [32,34,35], being its chemical synthesis much more economical than the whole protein [36] and possessing a greater physico-chemical stability. The selection of template epitopes for imprinted polymers must be carefully carried out taking into account the uniqueness of the sequence for the protein of interest, same structural configuration as in the native protein, length of about 8–20 amino acids and lacking of post-translational modifications [37].

In this work, we report the first example of electrochemical sensor for the detection of cardiac troponin T by using MIP-NGs as recognition elements. The MIP-NGs were produced by solid-phase synthesis in aqueous environment according to a previously reported protocol [38] by employing a protein epitope as template. The as-synthesized MIP-NGs were then anchored onto the surface of disposable screen-printed carbon electrodes exploiting the electrografting of 4-aminobenzoic acid (4-ABA) diazonium salt. Such anchoring procedure, although rarely applied [26], resulted in an easy and reliable MIP-NGs attachment to the electrode. The sensor performance resulted satisfactory in cTnT impedimetric detection both in phosphate buffer and undiluted serum. Remarkably, the sensor performance was comparable to that of high sensitive assays with a LOD of 0.004 ng/mL and the employment of disposable screen-printed electrodes, requiring a low sample volume without any modification [39], may contribute to the as-produced sensor to serve as an alternative detection tool for assessing cTnT in cardiac damage suspected clinical conditions with potential application at the POCT.

2. Materials and methods

2.1. Reagents and instruments

All chemicals were of analytical grade and purchased from Sigma-Aldrich, unless otherwise stated. The working solutions were prepared in ultra-pure water with a conductivity of <0.1 μS/cm. Phosphate buffer (0.1 M, pH 7) was prepared by mixing proper volumes of 0.5 M KH_2PO_4 and 0.5 M Na_2HPO_4. A solution of 5 mM $[Fe(CN)_6]^{3-/4-}$ was prepared in 50 mM phosphate buffer pH 7.4 with 0.1 M KCl as supporting electrolyte. The cTnT epitope template (CIDHLNEDQLC-K(N_3)), cyclized and modified with an azido terminal group, was custom synthesized by GenScript (New Jersey, USA). Recombinant human cardiac troponin T type 2 (TNNT2, MW = 37 kDa, pI = 4.88) was purchased from Tebubio (France, Europe). Proteins tested as potential interferents, namely human serum albumin (HSA, MW = 66.5 kDa, pI = 4.7), human hemoglobin (HHb, MW = 64.5 kDa, pI = 7.2) and human insulin (Ins, MW = 5.8 kDa, pI = 5.3), and human serum were purchased from Sigma-Aldrich. Screen-printed carbon electrodes (C-SPEs, DRP-11 L), equipped with carbon working and auxiliary electrodes and silver/silver chloride pseudoreference electrode, were purchased by Metrohm DropSens (Switzerland). Electrochemical measurements were carried out on PalmSens4 Potentiostat integrated with PSTrace software (Netherlands).

2.2. Electrode functionalization with MIP-NGs against cTnT

Molecularly imprinted nanogels against cTnT were produced by solid-phase synthesis employing the epitope CIDHLNEDQLC-K(N3) (C—C cyclic) as template, according to a protocol published earlier

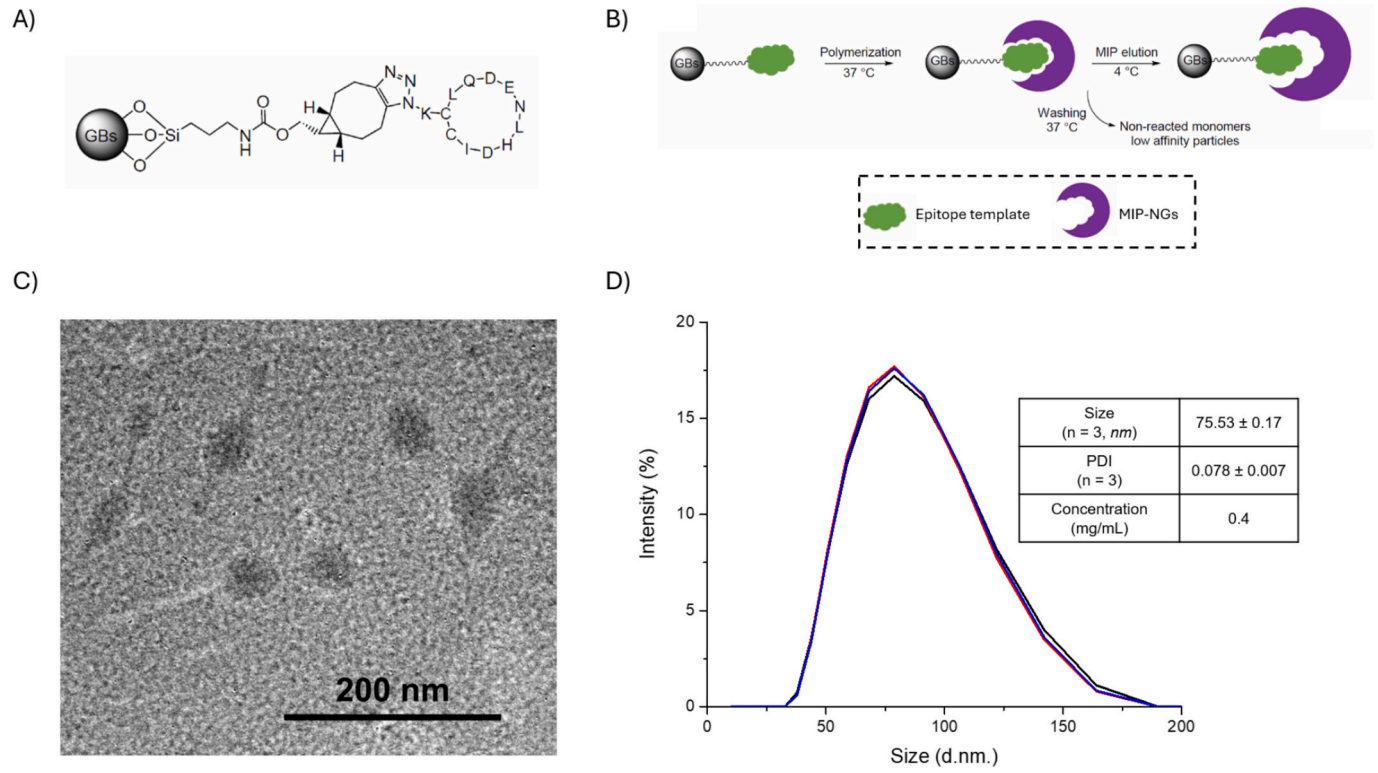

Fig. 1. Synthesis and morphological characterization of cTnT MIP-NGs. A) Epitope imprinting and B) solid-phase synthesis of cTnT MIP-NGs (Adapted from [38]). C) TEM and D) DLS analysis results of cTnT MIP-NGs morphological characterization (inset: hydrodynamic size of MIP-NGs, PDI index and MIP-NGs concentration).

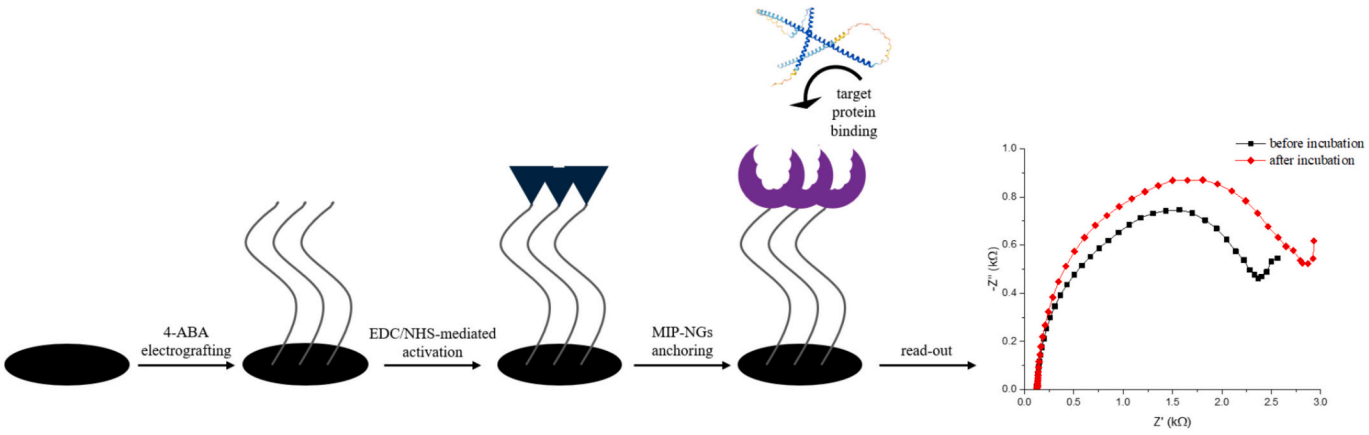

Fig. 2. Schematization of the stepwise fabrication of cTnT impedimetric sensor based on MIP-NGs.

[38], with slight modifications. The monomer composition and concentration of polymerization mixture (Table S1), as well as TEM and DLS characterization parameters for the morphological characterization of cTnT MIP-NGs, are reported in SI. The electrode functionalization and subsequent MIP-NGs anchoring protocol onto commercial screen-printed carbon electrodes were adapted from reference literature [26,40], exploiting the electrografting of 4-aminobenzoic acid diazonium salt in order to provide the electrode surface with carboxyl groups. MIP-NGs were anchored onto the electrode surface by reacting with the diazonium salt carboxyl groups through EDC/NHS mediation. The same electrode surface modification protocol was employed for the anchoring of MIP-NGs synthesized against a TNF-α epitope [30] and used as control to the assess the specific binding of the target protein, hence referred to as CONT-NGs. More details regarding the electrode functionalization are provided in SI. The modified electrodes were stored in a Petri dish under ambient laboratory conditions without any specific storage precautions, before the use.

2.3. *Target binding and selectivity tests*

The target binding on MIP-NGs and the sensor selectivity were assessed by exposing the functionalized sensors to increasing concentrations of either cTnT epitope, whole target protein or interferents for 30 min at 37 °C. Afterwards, the impedimetric signal was recorded. Further information about target binding and selectivity test are provided in SI.

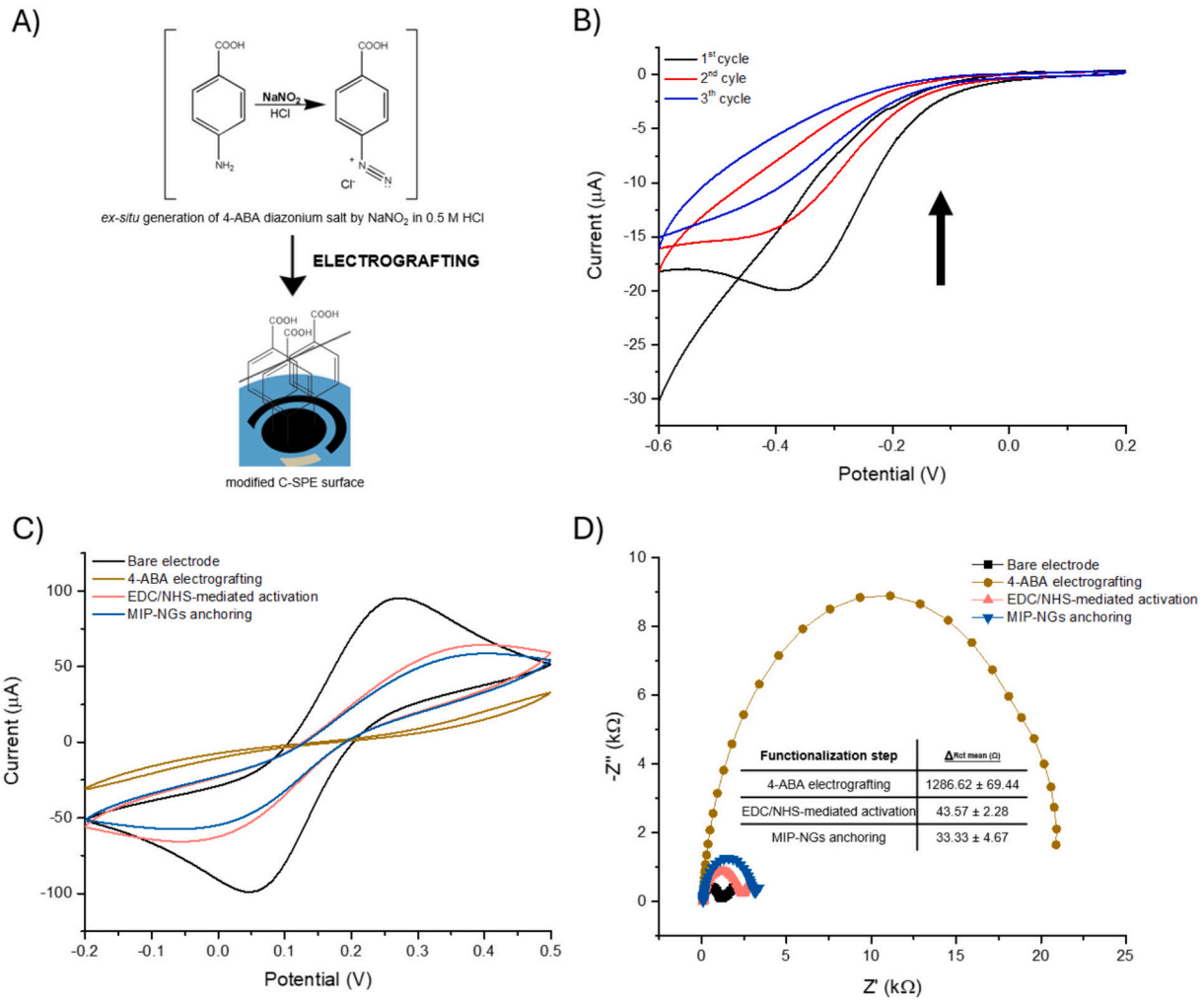

Fig. 3. Electrode functionalization. A) Schematic representation of C-SPE surface modification by 4-ABA diazonium salt electrografting, which comprised the *ex-situ* generation of 4-ABA diazonium salt by reaction with $NaNO_2$ in 0.5 M HCl and the diazonium salt electrografting, resulting in the formation of an organic layer exposing carboxyl groups onto the C-SPE surface. B) CV curves of 4-ABA electrografting. C) CV curves and D) EIS spectra of electrode functionalization in 5 mM $[Fe(CN)_6]^{3-/4-}$ (inset: ΔRct mean values for the functionalization steps, $n = 3$).

2.4. Real sample analysis

The sensor was also tested in real sample, by exposing it to undiluted serum spiked with increasing concentrations of cTnT (0.01–0.3 ng/mL) for 30 min at 37 °C. The sensor was then rinsed with deionized water and dried with a gentle stream of nitrogen before performing the electrochemical measurements. Further information about recovery percentage calculation can be found in SI.

3. Results and discussion

3.1. MIP-NGs morphological characterization

The solid-phase synthesis protocol of MIP-NGs specific for an epitope of cTnT was adapted from published literature [38] and comprised the peptide CIDHLNEDQLC (C—C cyclic) as the template (Fig. 1A and B). The as-synthesized MIP-NGs were morphologically characterized by TEM (Fig. 1C) and DLS analysis (Fig. 1D), which coherently revealed a nanometric size of MIP-NGs of about 75 nm with a narrow particle size distribution, as demonstrated by the low polydispersity index (PDI), equals to 0.078 ($n = 3$), which also remarked the reproducibility of the synthetic strategy.

3.2. Electrode functionalization

The as-synthetized MIP-NGs, bearing selective binding sites mostly at the polymer surface, were employed as recognition element, while screen-printed carbon electrodes (C-SPEs) with a three-electrode configuration were used for MIP-NGs anchoring upon surface modification. Fig. 2 reports a comprehensive schematization of the proposed cTnT sensor fabrication.

Recently, the modification of carbon surfaces by means of the electrografting of diazonium salts was shown to be a powerful technique providing a layer for the covalent immobilization of biomolecules. The strategy consists in the formation of aryl radicals by electrochemical reduction of diazonium salts deriving from aromatic amines and their subsequent covalent bonding with the electrode surface. The result is the establishment of an organic layer on the electrode surface exposing suitable functionalities that can be further exploited for the covalent immobilization of molecules [26,41,42]. Interestingly, several works demonstrated the great efficacy of electrografting for the electrode surface modification over other procedures for biomolecule immobilization, such as the self-assembly monolayer (SAM) formation on gold electrodes, commonly based on the chemisorption of thiols and amines, which could result in variable and low yield layers [43]. In this work, the electrografting protocol firstly involved the *ex-situ* generation of 4-ABA diazonium salt (Fig. 3A), generally known as diazotization reaction,

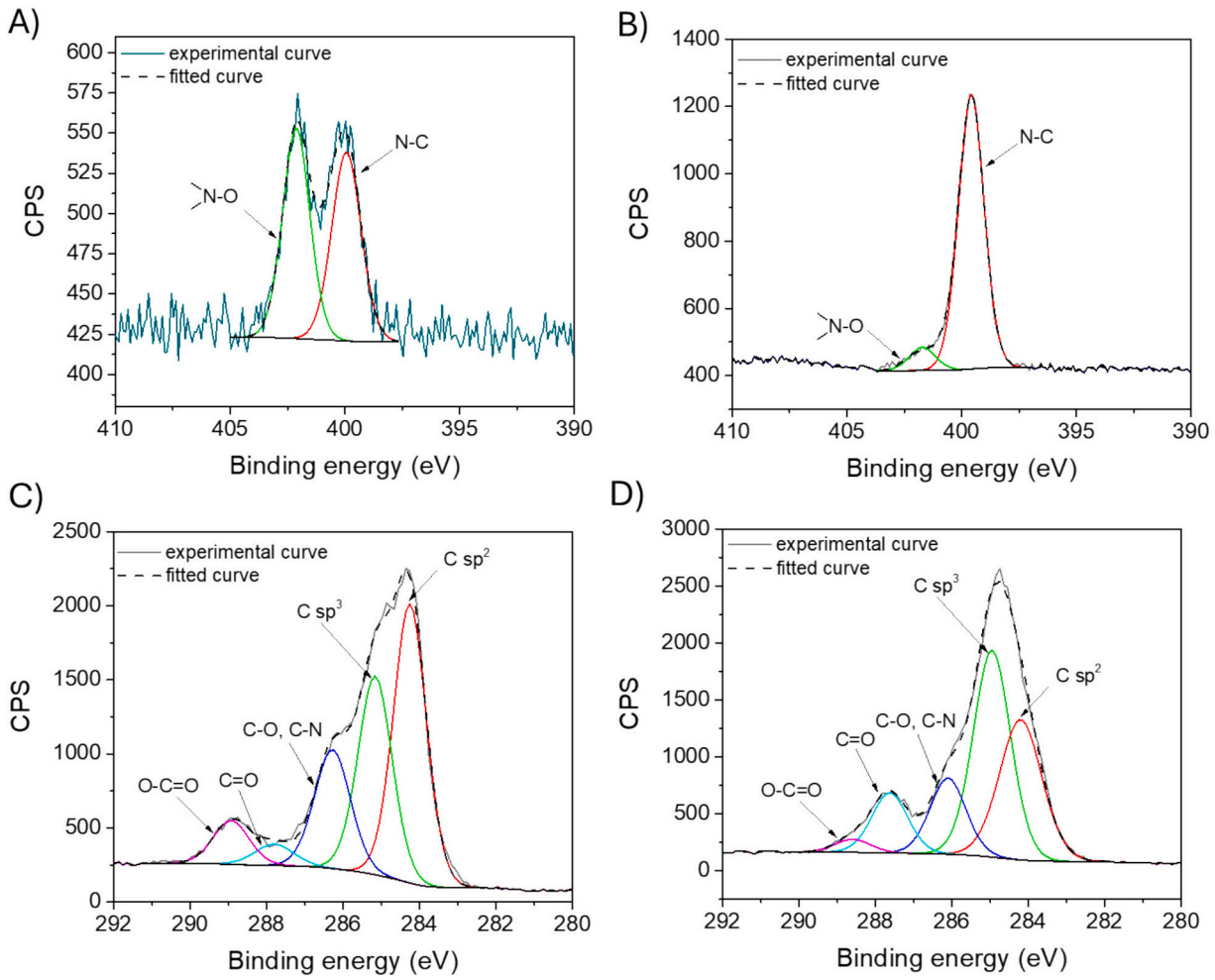

Fig. 4. XPS characterization. A) High-resolution spectra of N 1 s signal recorded after 4-ABA electrografting and EDC/NHS activation and B) MIP-NGs anchoring onto the electrode surface. C) High-resolution C 1 s spectrum recorded after the EDC/NHS activation step and D) MIP-NGs anchoring onto the electrode surface.

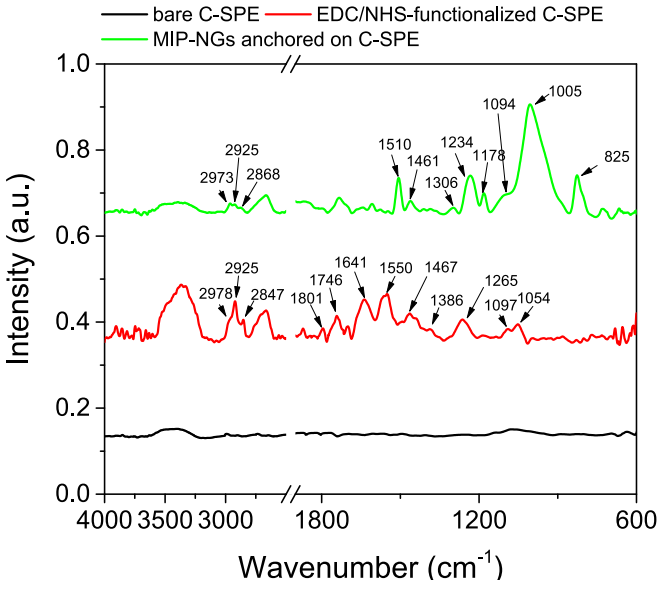

Fig. 5. FTIR characterization of C-SPE functionalization. FTIR spectra recorded for: bare electrode (black line); EDC/NHS-functionalized C-SPE (red line); MIP-NGs anchored onto C-SPE surface (green line). (For interpretation of the references to colour in this figure legend, the reader is referred to the web version of this article.)

where the primary aromatic amine reacted with sodium nitrite in a strong acidic environment, converting the nitrogen group into a diazonium functionality [44]. During the cyclic voltammetry, where the diazonium salt reduction occurred, the first scan showed a well-defined cathodic peak around −0.4 V (Fig. 3B), which progressively disappeared, suggesting the formation of a passivating carboxyphenyl layer [45,46]. Subsequentially, MIP-NGs anchoring was achieved by exploiting the EDC/NHS mediation [47].

CV characterization in $[Fe(CN)_6]^{3-/4-}$ was employed to observe the faradic current changes upon electrode functionalization (Fig. 3C). According to literature, the 4-ABA electrografting resulted in the electrode surface modification by means of an organic layer exposing negatively charged carboxyl groups, acting as an electrostatic barrier which repelled the negatively charged redox probe. Therefore, upon electrografting the redox probe electroactivity was dramatically decreased compared to the bare electrode, as expected [48]. The 4-ABA carboxyl group activation mediated by EDC/NHS restored the redox probe faradic currents due to the neutralization of surface-exposed negative charges [49]. Finally, the MIP-NGs anchoring onto the electrode surface slightly decreased the faradic currents, due to the nonconductive nature of polyNIPAM-based nanogels [50,51]. Overall, the CV results confirmed the successful electrode surface modification.

EIS characterization in $[Fe(CN)_6]^{3-/4-}$ provided more insights into the electrode surface modification towards MIP-NGs anchoring (Fig. 3D), by observing the semicircle changes from the Nyquist plot obtained in the selected frequency range [52]. Compared to the bare

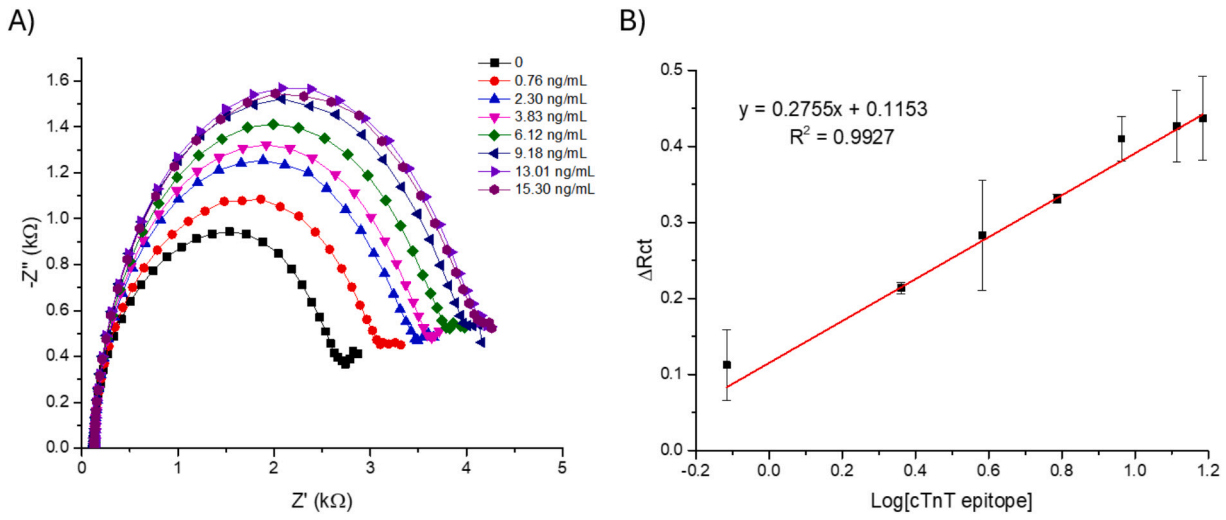

Fig. 6. Sensor response towards the cTnT epitope template. A) EIS spectra in $[Fe(CN)_6]^{3-/4-}$ of sensor response towards increasing concentrations of cTnT epitope template in phosphate buffer. B) Calibration curve of sensor response towards cTnT epitope in phosphate buffer.

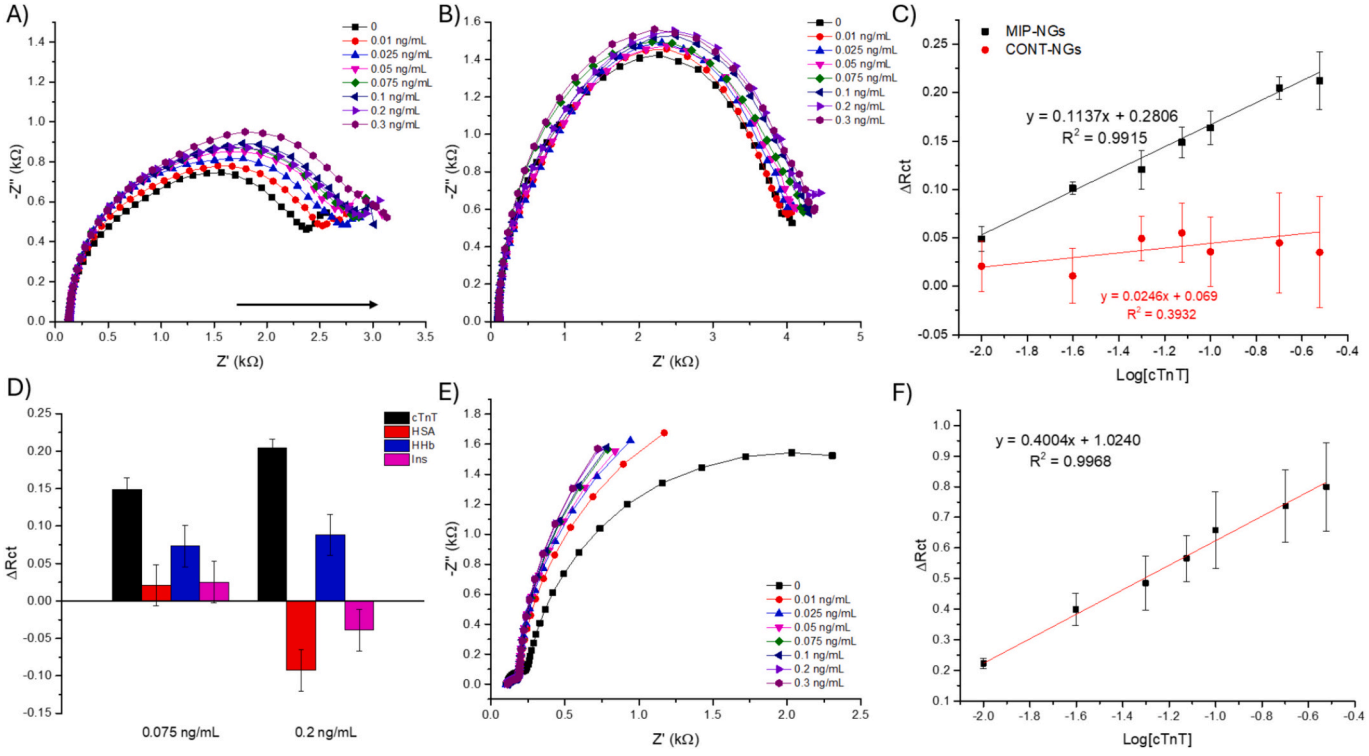

Fig. 7. Analytical characterization of cTnT sensor functionalized with MIP-NGs. A) EIS spectra of sensor response towards increasing concentrations of cTnT whole protein in phosphate buffer. B) EIS spectra of the sensor functionalized with CONT-NGs towards increasing concentrations of cTnT whole protein in phosphate buffer. C) Calibration curve of ΔRct as function of cTnT concentration logarithm. For comparison, the calibration curve for CONT-NGs response towards cTnT is reported. D) Sensor response towards interfering proteins with respect to cTnT. E) EIS spectra of MIP-NGs sensor response in undiluted serum spiked with increasing concentrations of cTnT protein. F) Calibration curve of sensor response towards increasing concentrations of cTnT whole protein in undiluted serum.

Table 1
Recovery percentages of cTnT spiked undiluted serum.

[cTnT] added (ng/mL)	[cTnT] estimated (ng/mL)	Recovery (%)
0.01	0.012	122.3 ± 0.06
0.075	0.088	117.59 ± 0.16
0.3	0.338	112.74 ± 0.22

electrode, the diazonium salt electrografting drastically increased the semicircle diameter, and thus the charge transfer resistance, due to the repulsion between the negative charges of 4-ABA carboxyl groups, exposed by the electrode surface upon electrografting, and the negatively charged redox probe [53]. The EDC/NHS-mediated activation of carboxyl groups decreased the impedance due to the neutral charges of NHS-ester that allow the electron transfer between the solution and the electrode surface [54]. Finally, as aforementioned, the nonconductive nature of polyNIPAM-based nanogels slightly increased the charge transfer resistance, thus confirming the CV results. The EIS signal on

Table 2
MIP-based electrochemical sensors for cTnT detection.

Functional monomer(s)	Transducer	Technique	Concentration range	LOD	Real sample	Ref.
o-PD	Gold electrode	CV	0.009–0.8 ng/mL	9 pg/mL	Diluted human serum	[64]
Py and carboxylated derivatives	RGO-modified SPE	DPV	0.01–0.1 ng/mL	0.006 ng/mL	Diluted human serum	[65]
ANI and carboxylated derivatives	Graphite SPE	DPV	0.02–0.09 ng/mL	0.008 ng/mL	Diluted human serum	[66]
o-PD	Gold electrode on $Si_3N_4/SiO_2/Si$ substrate	LSV	0.017–10 ng/mL	0.017 ng/mL	Human serum	[8]
ANI	MWCNTs/PMB-modified carbon SPE	DPV	0.10–8 pg/mL	0.040 pg/mL	Human plasma	[67]
o-PD	Silicon wafer	LSV	<0.03 ng/mL	5.34 pg/mL	Human serum	[68]
MIP-NGs	**Carbon SPE**	**EIS**	**0.01–0.3 ng/mL**	**0.004 ng/mL**	**Human serum**	**This work**

MIP-NGs-modified electrode has been acquired after the electrode assembly and after 3-days storage at ambient conditions. The high similarity of the two signals, with a variation of only 1.7%, confirmed the storage stability of the device prior to its use.

3.3. X-ray photoelectron spectroscopy (XPS) characterization

XPS was employed to monitor the surface chemistry of the electrode bearing MIP-NGs, making a comparison with the system before nanogels anchoring. Results are reported in Fig. 2, showing detailed C 1 s and N 1 s spectra recorded at both steps. N 1 s spectrum on the electrode after 4-ABA electrografting and EDC/NHS activation (Fig. 4A) exhibits two distinct components, one at 399.8 ± 0.2 eV, attributed to neutral amino groups, and another one at 402.0 ± 0.2 eV, consistent with oxidized nitrogen (>N–O) functionalities formed through the reaction between NHS and 4-ABA mediated by EDC. Upon MIP-NGs anchoring (Fig. 4B), a marked increase in N–C/N-H species was observed, evidently due to the abundance of not oxidized nitrogen species in the nanogels structure. Remarkably, the ratio between the two N1s components increased from 1.06 ± 0.06 to 11.9 ± 0.2 when comparing the system before and after MIP-NGs anchoring.

High-resolution C 1 s spectra further supported the successful modification of the electrode surface. After the EDC/NHS activation step (Fig. 4C), C 1 s signal presented a major peak at 284.2 ± 0.1 eV – ascribable to sp^2 carbon due to the graphitic carbon-based electrode and aromatic rings of 4-ABA molecule – a peak at 284.9 ± 0.1 eV from aliphatic carbon and three additional peaks at higher binding energy ascribed to oxidized carbon species, namely C–O/C–N at 286.0 ± 0.1 eV, carbonyl (C=O) signal at ~287.7 eV and carboxylate (O–C=O) component at ~288.6 eV. On samples bearing MIP-NGs (Fig. 4D), the decrease of sp^2 carbon peak can be observed, possibly suggesting a major coverage of the electrode surface, along with a slight increase of C=O component, likely reflecting the presence of monomeric units rich in these functionalities. XPS results thus indirectly confirmed the successful MIP-NGs anchoring to the electrode surface, corroborating the electrochemical characterization. Moreover, the high reproducibility observed intra-electrode (~2.5%) suggested the homogeneous surface modification and the reliability of the MIP-NGs anchoring strategy adopted.

3.4. Fourier transform infrared (FTIR) spectroscopy characterization

FTIR spectroscopy confirmed the stepwise surface modification of the C-SPE (Fig. 5). After electrografting with 4-aminobenzoic acid and subsequent EDC/NHS-mediated activation, several new absorption bands emerged, indicating the formation of activated carboxyl-derived species. In particular, the appearance of bands at 1746 cm^{-1} and ~1800 cm^{-1}, absent on the bare C-SPE, could be ascribed to symmetric and asymmetric stretching of the NHS ester carbonyl groups [55]. Other features at 1641 cm^{-1} and 1550 cm^{-1} can be attributed to amide-type vibrational modes, commonly associated with C=O stretching (amide I) and N—H bending coupled with C—N stretching (amide II). All these features are widely reported in FTIR studies of carbodiimide-activated carboxyl groups and amide bond formation following EDC/NHS chemistry, even prior to final coupling with nucleophilic amines, due to the presence of NHS esters and transient amide-like intermediates [55,56]. The broad absorption band between 3200 and 3600 cm^{-1} is attributed to overlapping N—H and O—H stretching vibrations, indicative of hydrogen-bonded amide-related groups and surface hydroxyls formed upon activation in aqueous conditions [55,56].

Upon immobilization of MIP-NGs, the FTIR spectrum (Fig. 5, green trace) closely matches that of MIP-NGs directly cast onto the ATR crystal (Fig. S1), particularly in the 1005–1175 cm^{-1} region, where the characteristic broad polymer band is observed. This strong spectral similarity provides clear evidence of successful electrode functionalization with MIP-NGs. In addition, features at 1234 cm^{-1} are consistent with amide III bands involving combined C—N stretching and N—H bending typical of polyacrylamide polymers. Absorptions in the 1460–1470 cm^{-1} region are consistent with CH_2 bending and C—H deformation of alkyl side chains. The band at ~1510 cm^{-1} corresponds to additional amide II contributions from the nanogel network, confirming the presence of covalently anchored polymer chains. Additional absorptions from 2868 to 2973 cm^{-1} may be related to stretching vibration of methyl groups within the complex polymer network. The persistence of the broad O–H/N–H stretch indicates hydrated polymer and surface functionalities remain after nanogel attachment [57–59]. Overall, the evolution of characteristic amide and polymer vibrational signatures strongly supports successful surface activation and covalent immobilization of MIP-NGs onto C-SPEs.

3.5. Target protein detection

The MIP-NGs sensor analytical features were first evaluated towards the cTnT epitope detection (Fig. 6). The electrode was incubated with phosphate buffer containing increasing concentrations of the epitope at 37 °C, temperature selected to promote the interaction between MIP-NGs and the target, being used during nanogels synthesis. During the investigation process, two different incubation times were tested, namely 15 and 30 min. Since a 30 min incubation time resulted in a higher sensor response, it was selected for target rebinding. The semicircle diameter increased at cTnT epitope increasing concentrations (Fig. 6A), indicating that more cavities were progressively occupied by the target, therefore reducing the electron transfer between the redox probe and the electrode at the interface and increasing the charge transfer resistance, a phenomenon known as gate effect [60]. The EIS spectra were fitted with the equivalent circuit reported in Fig. S2A and comprising Rsol as the electrolyte resistance, Rct as the charge transfer resistance in series with the Warburg impedance (W) for diffusion phenomena and both in parallel with CPE as constant phase element for non-ideal systems. The semicircle diameter increase was correlated with the progressive increase of Rct, which was extracted and processed according to Eq. 1, thus obtaining the ΔRct. By plotting ΔRct as function of cTnT epitope concentration logarithm (Fig. 6B), a sensor linear response in the concentration range 0.76–15.30 ng/mL (R^2 = 0.9927) was observed. The regression equation can be expressed as y = (0.2755 ± 0.0105)x log [cTnT epitope] + (0.1153 ± 0.0071). The relative standard deviation (RSD%, $n = 3$), calculated for 6.12 ng/mL, which was in the middle of the calibration curve, was 1.74%, thus indicating a highly

accurate target epitope detection [3]. The limit of detection, according to Eq. 2 (reported in SI), and the limit of quantification, calculated from Eq. 3 (reported in SI), were 0.29 and 0.87 ng/mL, respectively.

Afterwards, freshly-prepared sensors were exposed to increasing concentrations of cTnT whole protein in phosphate buffer in the same experimental conditions (Fig. 7). As for the epitope detection, the semicircle diameter progressively increased (Fig. 7A), while the sensor functionalized with CONT-NGs presented a slight response towards cTnT increasing concentrations (Fig. 7B), as expected. By plotting ΔRct as function of cTnT whole protein concentration logarithm, a linear response for the MIP-NGs sensor was observed in the concentration range 0.01–0.3 ng/mL, corresponding to 0.27–8.11 pM ($R^2 = 0.9915$) (Fig. 7C), with a satisfactory reproducibility at 0.075 ng/mL (2.03 pM, RSD% = 10.65%), proving an accurate protein detection as requested by the guidelines [3]. The regression equation can be expressed as $y = (0.1137 \pm 0.0047)x \log [cTnT] + 0.2806 \pm 0.0068$. The limit of detection and the limit of quantification were equals to 0.004 ng/mL and 0.013 ng/mL, respectively, in total agreement with hs-cTnT assay values [11]. By comparing the sensor response (*i.e.*, ΔRct) towards the epitope and the whole protein, a correlation coefficient of 0.9774 was recorded (Fig. S3), which proved the sensor ability to detect both targets further validating the imprinting process. The imprinting factor (IF), calculated as the ratio between the slope of the MIP-NGs calibration curve and the slope of the CONT-NGs calibration curve ($IF = \text{slope}_{\text{MIP-NGs}} / \text{slope}_{\text{CONT-NGs}}$) was 4.62, thus confirming the efficacy of the imprinting process. A comprehensive table regarding the sensor analytical performance metrics is reported in SI (Table S2).

3.6. Selectivity and real sample analysis

The sensor selectivity was tested towards potential cTnT interfering serum proteins, such as HSA, HHb and Ins, at different concentrations (0.075 and 0.2 ng/mL, corresponding to 1.13 and 3.01 pM for HSA, 1.16 and 3.10 pM for HHb and to 12.93 and 34.48 pM for Ins, respectively). Overall, the sensor showed a negligible response towards the interfering agents (Fig. 7D), although in some cases a negative signal was recorded, most probably due to an adsorption of the molecule onto the electrode surface. A comprehensive table summarizing the sensor selectivity performance is reported in Table S3.

The MIP-NGs-based sensor performance was also tested in real sample upon exposure to undiluted serum spiked with increasing concentrations of the protein. A significantly different sensor response was observed (Fig. 7E), likely due to the complexity of the matrix, with the Nyquist plots comprising a small semicircle in the middle frequency region and a larger and incomplete semicircle at lower frequencies. Such sensor behaviour resulted to be well fitted ($\chi^2 < 0.002$) by a different equivalent circuit (Fig. S2B) made up of two series-connected circuits. Specifically, Rsol, representing the resistance of the electrolyte solution, is in series with a block including Rct as the charge transfer resistance in parallel with a capacitor (C), which described the small semicircle at middle frequencies. The additional block required for the fitting comprised Rα, a resistive component, and CPE, which expressed the larger semicircle in the low frequency region and indicated a rough and non-homogeneous surface, thus behaving as a non-ideal system. Results obtained from circuit fitting (Table S4) clearly revealed that Rsol did not show any remarkable change at increasing concentrations of cTnT protein, while Rct and C increased due to the progressive target protein binding to the imprinted sites at the interface. Additionally, Rα decreased and CPE increased and such behaviour was attributed to the accumulation of the redox probe negative charges onto the electrode, either by adsorption or electrostatic interactions [61–63]. In our hypothesis, as the target protein progressively bound to the binding sites of MIP-NGs (Rct/C), as expected, the serum components somehow affected the sensor surface and, consequently, the processes between the redox probe and the sensor (Rα/CPE).

As in the study of sensor response in phosphate buffer, Rct was employed as analytical parameter and processed as in Eq. 1. A linear response in undiluted serum spiked with the target protein was then observed in the same concentration range as phosphate buffer ($R^2 = 0.9968$) (Fig. 7F). By comparing the sensor responses in serum and in phosphate buffer, a correlation coefficient of 0.9967 was obtained (Fig. S4). From tests in spiked serum sample, recovery percentage was estimated. As reported in Table 1 (displaying percentage recoveries for three cTnT concentrations), satisfactory recovery values were achieved, demonstrating the reliability of the sensor performance in a complex real matrix.

Table 2 reports previous works about the development of electrochemical sensors based on molecularly imprinted polymers for the detection of cTnT.

4. Conclusions

In this work, molecularly imprinted nanogels towards a cardiac cell damage biomarker, namely cardiac troponin T (cTnT), synthesized by solid-phase synthesis in aqueous environment employing the epitope imprinting approach, were anchored onto the surface of disposable screen-printed carbon electrodes preliminary modified by 4-ABA diazonium salts electrografting. A detailed analysis either by CV and EIS in $[Fe(CN)_6]^{3-/4-}$ and by XPS and FT-IR characterization assessed the electrode functionalization. The MIP-NGs sensor showed a linear and accurate response towards the target protein in the concentration range 0.01–0.3 ng/mL, with a LOD of 0.004 ng/mL, in agreement with the limit of detection reported for high sensitive cTnT assays. Moreover, a negligible response was recorded towards some interfering proteins, along with a linear response towards the protein in serum. To the best of our knowledge, this work reported the first electrochemical sensor for cTnT detection based on MIP-NGs obtained by solid-phase synthesis *via* epitope imprinting approach. The system presented analytical performances comparable to commercially available immunoassays, with additional key advantages such as the environmental friendly synthesis of MIP-NGs, the more affordable employment of a protein epitope instead of the whole protein and the possible miniaturization of the low-volume sensing device. These features, along with sensor ability to detect cTnT in undiluted serum, showed the striking potential application of the developed sensor in the rapid and selective myocardial damage biomarker detection, providing a valid alternative to the common analytical techniques for cardiac troponin T detection.

CRediT authorship contribution statement

Francesco Gagliani: Writing – original draft, Methodology, Investigation, Conceptualization. **Tiziano Di Giulio:** Writing – original draft, Methodology, Investigation. **Muhammad Ibrar Asif:** Methodology, Investigation. **Noel Angelo Kalacas:** Methodology, Investigation. **Claudia Herrera-León:** Methodology, Investigation. **Alessia Di Fiore:** Methodology, Investigation. **Serena Laschi:** Resources, Methodology. **Francesco Ranaldi:** Resources, Methodology. **Paola Faraoni:** Resources, Methodology. **Gabriele Giancane:** Writing – review & editing, Visualization, Methodology, Investigation. **Cosimino Malitesta:** Methodology, Funding acquisition, Conceptualization. **Karsten Haupt:** Writing – review & editing, Supervision, Project administration, Funding acquisition. **Elisabetta Mazzotta:** Writing – review & editing, Supervision, Project administration, Funding acquisition.

Declaration of competing interest

The authors declare that they have no known competing financial interests or personal relationships that could have appeared to influence the work reported in this paper.

Acknowledgements

This work was funded by EU-Next Generation EU, Missione 4 Componente 1 CUP F53D23008850001, within the Project PRIN 2022 PNRR "HYbrid DEvices and mAchine Learning for food and environmental safety – **HYDEAL4safety**" (P2022T3HFA), by EU- Next Generation EU Project PRIN 2022 CUP F53D23004540006 "Smart diagnostic devices based on integrated 2D-nanomaterials and molecularly imprinted polymers (**2DnanoMIP**) (2022T2E7NT) and by the POS Salute 2014-2020 of the Italian Ministry of Health, under Trajectory 3 "Regenerative, Predictive and Personalized Medicine", Action Line 3.1, within the project "Integrated Health and Genetics System for Cardiovascular Diseases (SISAGEN-CARDIO)" (local project code T3-AN-18). Karsten Haupt acknowledges financial support from the French National Research Agency ANR (project **DynaBio**), and from Institut Universitaire de France.

Appendix A. Supplementary data

Supplementary data to this article can be found online at https://doi.org/10.1016/j.microc.2026.117793.

Data availability

Data will be made available on request.

References

[1] R. Ragusa, C. Caselli, Focus on cardiac troponin complex: from gene expression to cardiomyopathy, Genes Dis. 11 (2024) 101263, https://doi.org/10.1016/j.gendis.2024.101263.
[2] J. Osredkar, A. Bajrić, H. Možina, L. Lipar, A. Jerin, Cardiac troponins I and T as biomarkers of cardiomyocyte injury—advantages and disadvantages of each, Appl. Sci. 14 (2024) 6007, https://doi.org/10.3390/app14146007.
[3] A. Michailovich Chaulin, Diagnostic role and methods of detection of cardiac troponins: an opinion from historical and current points of view, Curr. Cardiol. Rev. 19 (2022) 10–20, https://doi.org/10.2174/1573403x18666220610164946.
[4] M. Pedrero, S. Campuzano, J.M. Pingarrón, Electrochemical biosensors for the determination of cardiovascular markers: a review, Electroanalysis 26 (2014) 1132–1153, https://doi.org/10.1002/ELAN.201300597.
[5] E.P.M. Cardinaels, A.M.A. Mingels, T. Van Rooij, P.O. Collinson, F.W. Prinzen, M. P. Van Dieijen-Visser, Time-dependent degradation pattern of cardiac troponin T following myocardial infarction, Clin. Chem. 59 (2013) 1083–1090, https://doi.org/10.1373/CLINCHEM.2012.200543.
[6] J. Dierkes, U. Domröse, S. Westphal, A. Ambrosch, H.P. Bosselmann, K. H. Neumann, C. Luley, Cardiac troponin T predicts mortality in patients end-stage renal disease, Circulation 102 (2000) 1964–1969, https://doi.org/10.1161/01.CIR.102.16.1964.
[7] T. Hayashi, T. Kimura, K. Yasuda, K. Sasaki, Y. Obi, H. Rakugi, Y. Isaka, Cardiac troponin T elevation at dialysis initiation is associated with all-cause and cardiovascular mortality on dialysis in patients without diabetic nephropathy, Clin. Exp. Nephrol. 21 (2017) 333–341, https://doi.org/10.1007/s10157-016-1278-4.
[8] P.S. Chen, Y.T. Lin, Y.T. Cheng, C.K. Lee, H.E. Tsai, Characterization and clinical serum test of a molecular imprinted polymer (MIP)-based cardiac troponin T sensing electrode for patient monitoring applications, J. Microelectromech. Syst. 29 (2020) 930–935, https://doi.org/10.1109/JMEMS.2020.3014397.
[9] P. Jarolim, High sensitivity cardiac troponin assays in the clinical laboratories, Clin. Chem. Lab. Med. 53 (2015) 635–652, https://doi.org/10.1515/cclm-2014-0565.
[10] F. Du, Y. Chen, C. Meng, B. Lou, W. Zhang, G. Xu, Recent advances in electrochemiluminescence immunoassay based on multiple-signal strategy, Curr. Opin. Electrochem. 28 (2021) 100725, https://doi.org/10.1016/j.coelec.2021.100725.
[11] R.Y. Xu, X.F. Zhu, Y. Yang, P. Ye, High-sensitive cardiac troponin T, J. Geriatr. Cardiol. 10 (2013) 102–109, https://doi.org/10.3969/j.issn.1671-5411.2013.01.015.
[12] K. Dhara, D.R. Mahapatra, Review on electrochemical sensing strategies for C-reactive protein and cardiac troponin I detection, Microchem. J. 156 (2020) 104857, https://doi.org/10.1016/J.MICROC.2020.104857.
[13] A.S. Streng, D. de Boer, W.P.T.M. van Doorn, J.M.M. Kocken, O. Bekers, W.K.W. H. Wodzig, Cardiac troponin T degradation in serum is catalysed by human thrombin, Biochem. Biophys. Res. Commun. 481 (2016) 165–168, https://doi.org/10.1016/J.BBRC.2016.10.149.
[14] A.M. Chaulin, L.S. Karslyan, E.V. Grigoriyeva, D.A. Nurbaltaeva, D.V. Duplyakov, Clinical and diagnostic value of cardiac markers in human biological fluids, Kardiologiia 59 (2019) 66–75, https://doi.org/10.18087/CARDIO.2019.11.N414.
[15] A. Campu, I. Muresan, A.M. Craciun, S. Cainap, S. Astilean, M. Focsan, Cardiac troponin biosensor designs: current developments and remaining challenges, Int. J. Mol. Sci. 23 (2022), https://doi.org/10.3390/ijms23147728.
[16] A. Dasgupta, A. Wahed, Cardiac markers, in: Clinical Chemistry, Immunology and Laboratory Quality Control, Second, Elsevier Inc., 2021, pp. 149–171.
[17] E. Antman, J.P. Bassand, W. Klein, M. Ohman, J.L. Lopez Sendon, L. Rydén, M. Simoons, M. Tendera, B.R. Chaitman, P. Clemmensen, E. Falk, M.C. Fishbein, M. Galvani, A.J. Garson, C. Grines, C. Hamm, U. Hoppe, A. Jaffe, H. Katus, J. Kjekshus, W. Klein, P. Klootwijk, C. Lenfant, D. Levy, R.I. Levy, R. Luepker, F. Marcus, U. Naslund, M. Ohman, O. Pahlm, P. Poole-Wilson, R. Popp, K. Pyorala, J. Ravkilde, N. Rehnquist, W. Roberts, R. Roberts, J. Roelandt, L. Ryden, S. Sans, M. L. Simoons, K. Thygesen, H. Tunstall-Pedoe, R. Underwood, B.F. Uretsky, F. Van de Werf, L.M. Voipio-Pulkki, G. Wagner, L. Wallentin, W. Wijns, D. Wood, Myocardial infarction redefined - a consensus document of the joint European Society of Cardiology/American College of Cardiology Committee f or the redefinition of myocardial infarction, J. Am. Coll. Cardiol. 36 (2000) 959–969, https://doi.org/10.1016/S0735-1097(00)00804-4.
[18] P. Kelíšková, O. Matvieiev, L. Janíková, R. Šelešovská, Recent advances in the use of screen-printed electrodes in drug analysis: a review, Curr. Opin. Electrochem. 42 (2023), https://doi.org/10.1016/j.coelec.2023.101408.
[19] A. Pourali, M.R. Rashidi, J. Barar, G. Pavon-Djavid, Y. Omidi, Voltammetric biosensors for analytical detection of cardiac troponin biomarkers in acute myocardial infarction, TrAC Trends Anal. Chem. 134 (2021) 116123, https://doi.org/10.1016/j.trac.2020.116123.
[20] Z. Li, A. Zhong, Electrochemical detection strategies for cardiovascular disease biomarkers: applications in troponin I and troponin T assays, Int. J. Electrochem. Sci. 19 (2024) 100675, https://doi.org/10.1016/j.ijoes.2024.100675.
[21] B. Tse Sum Bui, A. Mier, K. Haupt, Molecularly imprinted polymers as synthetic antibodies for protein recognition: the next generation, Small 19 (2023) 1–17, https://doi.org/10.1002/smll.202206453.
[22] M. Bompart, K. Haupt, C. Ayela, Micro and nanofabrication of molecularly imprinted polymers, Top. Curr. Chem. 325 (2012) 83–110, https://doi.org/10.1007/128_2011_308.
[23] V.L.V. Granado, M. Gutiérrez-Capitán, C. Fernández-Sánchez, M.T.S.R. Gomes, A. Rudnitskaya, C. Jimenez-Jorquera, Thin-film electrochemical sensor for diphenylamine detection using molecularly imprinted polymers, Anal. Chim. Acta 809 (2014) 141–147, https://doi.org/10.1016/J.ACA.2013.11.038.
[24] T. Alizadeh, S. Nayeri, S. Mirzaee, A high performance potentiometric sensor for lactic acid determination based on molecularly imprinted polymer/MWCNTs/PVC nanocomposite film covered carbon rod electrode, Talanta 192 (2019) 103–111, https://doi.org/10.1016/j.talanta.2018.08.027.
[25] R. D'Aurelio, I. Chianella, J.A. Goode, I.E. Tothill, Molecularly imprinted nanoparticles based sensor for cocaine detection, Biosensors 10 (2020) 1–13, https://doi.org/10.3390/bios10030022.
[26] J. McClements, P.M. Seumo Tchekwagep, A.L. Vilela Strapazon, F. Canfarotta, A. Thomson, J. Czulak, R.E. Johnson, K. Novakovic, P. Losada-Pérez, A. Zaman, I. Spyridopoulos, R.D. Crapnell, C.E. Banks, M. Peeters, Immobilization of molecularly imprinted polymer nanoparticles onto surfaces using different strategies: evaluating the influence of the functionalized Interface on the performance of a thermal assay for the detection of the cardiac biomarker troponin i, ACS Appl. Mater. Interfaces 13 (2021) 27868–27879, https://doi.org/10.1021/acsami.1c05566.
[27] D. Carboni, K. Flavin, A. Servant, V. Gouverneur, M. Resmini, The first example of molecularly imprinted nanogels with aldolase type I activity, Chem. Eur. J. 14 (2008) 7059–7065, https://doi.org/10.1002/chem.200800675.
[28] Y. Zhao, C. Simon, M. Daoud Attieh, K. Haupt, A. Falcimaigne-Cordin, Reduction-responsive molecularly imprinted nanogels for drug delivery applications, RSC Adv. 10 (2020) 5978–5987, https://doi.org/10.1039/c9ra07512g.
[29] A. Singhal, A. Singh, A. Shrivastava, R. Khan, Epitope imprinted polymeric materials: application in electrochemical detection of disease biomarkers, J. Mater. Chem. B 11 (2023) 936–954, https://doi.org/10.1039/D2TB02135H.
[30] C. Herrera León, N.A. Kalacas, A. Mier, P. Sakhaii, F. Merlier, E. Prost, I. Maffucci, V. Montagna, H. Mora-Radó, P.K. Dhal, B. Tse Sum Bui, K. Haupt, Synthetic peptide antibodies as TNF-α inhibitors: molecularly imprinted polymer nanogels neutralize the inflammatory activity of TNF-α in THP-1 derived macrophages, Angew. Chem. Int. Ed. 62 (2023), https://doi.org/10.1002/anie.202306274.
[31] J. Xu, S. Ambrosini, E. Tamahkar, C. Rossi, K. Haupt, B. Tse Sum Bui, Toward a universal method for preparing molecularly imprinted polymer nanoparticles with antibody-like affinity for proteins, Biomacromolecules 17 (2016) 345–353, https://doi.org/10.1021/acs.biomac.5b01454.
[32] P.X. Medina Rangel, S. Laclef, J. Xu, M. Panagiotopoulou, J. Kovensky, B. Tse Sum Bui, K. Haupt, Solid-phase synthesis of molecularly imprinted polymer nanolabels: affinity tools for cellular bioimaging of glycans, Sci. Rep. 9 (2019), https://doi.org/10.1038/S41598-019-40348-5.
[33] A. Poma, A. Guerreiro, M.J. Whitcombe, V. Elena, Solid-phase synthesis of molecularly imprinted polymer nanoparticles with a reusable template – " plastic antibodies", Adv. Funct. Mater. 23 (2016) 2821–2827, https://doi.org/10.1002/adfm.201202397.Solid-Phase.
[34] S. Ambrosini, S. Beyazit, K. Haupt, B. Tse Sum Bui, Solid-phase synthesis of molecularly imprinted nanoparticles for protein recognition, Chem. Commun. 49 (2013) 6746–6748, https://doi.org/10.1039/c3cc41701h.
[35] P. Palladino, M. Minunni, S. Scarano, Cardiac troponin T capture and detection in real-time via epitope-imprinted polymer and optical biosensing, Biosens. Bioelectron. 106 (2018) 93–98, https://doi.org/10.1016/j.bios.2018.01.068.

[36] S.P.B. Teixeira, R.L. Reis, N.A. Peppas, M.E. Gomes, R.M.A. Domingues, Epitope-imprinted polymers: design principles of synthetic binding partners for natural biomacromolecules, Sci. Adv. 7 (2021), https://doi.org/10.1126/sciadv.abi9884.
[37] A. Mier, I. Maffucci, F. Merlier, E. Prost, V. Montagna, G.U. Ruiz-Esparza, J. V. Bonventre, P.K. Dhal, B. Tse Sum Bui, P. Sakhaii, K. Haupt, Molecularly imprinted polymer nanogels for protein recognition: direct proof of specific binding sites by solution STD and WaterLOGSY NMR spectroscopies, Angew. Chem. Int. Ed. 60 (2021) 20849–20857, https://doi.org/10.1002/anie.202106507.
[38] C. Herrera-León, E.I. Paruli, C. Thomas, N.A. Kalacas, A. Di Fiore, G.P. Villezcas, A. Mier, R. Marquant, I. Maffucci, O. Soppera, C. Gonzato, B. Tse Sum Bui, K. Haupt, New coupling method for anchoring molecularly imprinted polymers onto polymeric transducers: a case study for the detection of the heart failure biomarker Troponin T, Polymer (Guildf.) 343 (2026) 129423. Contents, https://doi.org/10.1016/j.polymer.2025.129423.
[39] F. Gagliani, Giulio T. Di, S. Grecchi, T. Benincori, S. Arnaboldi, C. Malitesta, E. Mazzotta, Green synthesis of a molecularly imprinted polymer based on a novel Thiophene-derivative for electrochemical sensing, Molecules 29 (2024) 1632, https://doi.org/10.3390/molecules29071632.
[40] S. Eissa, M. Zourob, A graphene-based electrochemical competitive immunosensor for the sensitive detection of okadaic acid in shellfish, Nanoscale 4 (2012) 7593–7599, https://doi.org/10.1039/c2nr32146g.
[41] S. Abdellaoui, B.C. Corgier, C.A. Mandon, B. Doumèche, C.A. Marquette, L.J. Blum, Biomolecules immobilization using the aryl diazonium electrografting, Electroanalysis 25 (2013) 671–684, https://doi.org/10.1002/elan.201200334.
[42] P. Yáñez-Sedeño, S. Campuzano, J.M. Pingarrón, Integrated affinity biosensing platforms on screen-printed electrodes electrografted with diazonium salts, Sensors (Switzerland) 18 (2018), https://doi.org/10.3390/s18020675.
[43] W. Ma, Preparation and performance analysis of electrochemically assisted molecular electronic devices, Int. J. Electrochem. Sci. 19 (2024) 100489, https://doi.org/10.1016/j.ijoes.2024.100489.
[44] G. Roos, C. Roos, Functional classes II, reactions, in: Organic Chemistry Concepts, 2015, pp. 103–149, https://doi.org/10.1016/B978-0-12-801699-2.00007-9.
[45] I. Bakas, Z. Salmi, S. Gam-Derouich, M. Jouini, S. Lépinay, B. Carbonnier, A. Khlifi, R. Kalfat, F. Geneste, Y. Yagci, M.M. Chehimi, Molecularly imprinted polymeric sensings layers grafted from aryl diazonium-modified surfaces for electroanalytical applications. A mini review, Surf. Interface Anal. 46 (2014) 1014–1020, https://doi.org/10.1002/sia.5451.
[46] M. Chehimi, J. Pinson, F. Mousli, Aryl Diazonium Salts and Related Compounds Surface Chemistry and Applications, 2022.
[47] M.J.E. Fischer, Amine coupling through EDC/NHS: a practical approach, in: N. Mol, M. Fischer (Eds.), Surface Plasmon Resonance. Methods in Molecular Biology, Humana Press, 2010, pp. 55–73.
[48] L. Gillan, T. Teerinen, L.S. Johansson, M. Smolander, Controlled diazonium electrodeposition towards a biosensor for C-reactive protein, Sens. Int. 2 (2021) 100060, https://doi.org/10.1016/j.sintl.2020.100060.
[49] M. Moreno-Guzmán, A. González-Cortés, P. Yáñez-Sedeño, J.M. Pingarrón, Multiplexed ultrasensitive determination of Adrenocorticotropin and cortisol hormones at a dual electrochemical immunosensor, Electroanalysis 24 (2012) 1100–1108, https://doi.org/10.1002/elan.201200070.
[50] L.J. Zhang, L.F. Feng, X.P. Gu, C.L. Zhang, Electro-conductive and temperature-sensitive poly(N-isopropylacrylamide) composite hydrogels with improved mechanical properties, Appl. Nanosci. 10 (2020) 2189–2198, https://doi.org/10.1007/s13204-020-01358-2.
[51] Z. Deng, Y. Guo, X. Zhao, T. Du, J. Zhu, Y. Xie, F. Wu, Y. Wang, M. Guan, Poly(N-Isopropylacrylamide) based electrically conductive hydrogels and their applications, Gels 8 (2022) 280, https://doi.org/10.3390/gels8050280.
[52] H.S. Magar, R.Y.A. Hassan, A. Mulchandani, Electrochemical impedance spectroscopy (Eis): principles, construction, and biosensing applications, Sensors 21 (2021), https://doi.org/10.3390/s21196578.
[53] P.G. Wang, B.R. Li, Y.L. Wang, C.C. Wu, J.C. Chen, Application of aminobenzoic acid electrodeposited screen-printed carbon electrode in the beta-amyloid electrochemical impedance spectroscopy immunoassay, Talanta 254 (2023) 124154, https://doi.org/10.1016/j.talanta.2022.124154.
[54] C. Ocaña, A. Hayat, R.K. Mishra, A. Vasilescu, M. del Valle, J.L. Marty, Label free aptasensor for lysozyme detection: a comparison of the analytical performance of two aptamers, Bioelectrochemistry 105 (2015) 72–77, https://doi.org/10.1016/j.bioelechem.2015.05.009.
[55] M. Dogan, S. Nazir, D. Jenkins, Y. Wei, G. Pan, Electrochemical detection of Aβ42 and Aβ40 at Attomolar scale via optimised antibody loading on Pyr-NHS-functionalised 3D graphene foam electrodes, Biosensors 15 (2025) 1–18, https://doi.org/10.3390/bios15120806.
[56] S. Sam, L. Touahir, J.S. Andresa, P. Allongue, J. Chazalviel, C.H. De Villeneuve, A. Moraillon, F. Ozanam, N. Gabouze, S. Djebbar, Semiquantitative study of the EDC/NHS activation of acid terminal groups at modified porous silicon surfaces, Lang 26 (2010) 809–814, https://doi.org/10.1021/la902220a.
[57] P. Roach, D.J. Mcgarvey, M.R. Lees, C. Hoskins, Remotely triggered scaffolds for controlled release of pharmaceuticals, Int. J. Mol. Sci. 14 (2013) 8585–8602, https://doi.org/10.3390/ijms14048585.
[58] M. Ziaee, P. Zahedi, M. Abdouss, M.A. Zarandi, S. Manouchehri, N. Mozdoori, Electrospun poly (N-isopropylacrylamide-co-acrylic acid)/cellulose laurate blend nanofibers containing adapalene: morphology, drug release, and cell culture studies, Int. J. Polym. Mater. Polym. Biomater. 65 (2016) 477–486, https://doi.org/10.1080/00914037.2015.1129961.
[59] T. Xiao-liang, G.U.O. Shao-meng, L.I.U. Zi-dian, T. Ren-zhi, P. Jia-yu, C. Yang, Preparation of thermo-sensitive poly (N-isopropylacrylamide) film using KHz alternating current dielectric barrier discharge, in: Proceedings of the 2017 3rd International Forum on Energy, Environment Science and Materials (IFEESM 2017), 2018, pp. 598–602.
[60] P.S. Sharma, A. Garcia-Cruz, M. Cieplak, K.R. Noworyta, W. Kutner, 'Gate effect' in molecularly imprinted polymers: the current state of understanding, Curr. Opin. Electrochem. 16 (2019) 50–56, https://doi.org/10.1016/j.coelec.2019.04.020.
[61] N.R. Shanmugam, S. Muthukumar, S. Prasad, Ultrasensitive and low-volume point-of-care diagnostics on flexible strips-a study with cardiac troponin biomarkers, Sci. Rep. 6 (2016), https://doi.org/10.1038/SREP33423.
[62] A. Terbouche, S. Lameche, C. Ait-Ramdane-Terbouche, D. Guerniche, D. Lerari, K. Bachari, D. Hauchard, A new electrochemical sensor based on carbon paste electrode/Ru(III) complex for determination of nitrite: electrochemical impedance and cyclic voltammetry measurements, Meas J. Int. Meas Confed 92 (2016) 524–533, https://doi.org/10.1016/j.measurement.2016.06.034.
[63] F. Zouaoui, S. Bourouina-Bacha, M. Bourouina, A. Alcacer, J. Bausells, N. Jaffrezic-Renault, N. Zine, A. Errachid, Electrochemical impedance spectroscopy microsensor based on molecularly imprinted chitosan film grafted on a 4-Amino-phenylacetic acid (CMA) modified gold electrode, for the sensitive detection of glyphosate, Front. Chem. 9 (2021) 1–11, https://doi.org/10.3389/fchem.2021.621057.
[64] N. Karimian, M. Vagin, M.H.A. Zavar, M. Chamsaz, A.P.F. Turner, A. Tiwari, An ultrasensitive molecularly-imprinted human cardiac troponin sensor, Biosens. Bioelectron. 50 (2013) 492–498, https://doi.org/10.1016/j.bios.2013.07.013.
[65] B.V.M. Silva, B.A.G. Rodríguez, G.F. Sales, M.D.P.T. Sotomayor, R.F. Dutra, An ultrasensitive human cardiac troponin T graphene screen-printed electrode based on electropolymerized-molecularly imprinted conducting polymer, Biosens. Bioelectron. 77 (2016) 978–985, https://doi.org/10.1016/J.BIOS.2015.10.068.
[66] M. Karimi, M. Rabiee, M. Tahriri, R. Salarian, L. Tayebi, A graphene based–biomimetic molecularly imprinted polyaniline sensor for ultrasensitive detection of human cardiac troponin T (cTnT), Synth. Met. 256 (2019) 116136, https://doi.org/10.1016/j.synthmet.2019.116136.
[67] K. Phonklam, R. Wannapob, W. Sriwimol, P. Thavarungkul, T. Phairatana, A novel molecularly imprinted polymer PMB/MWCNTs sensor for highly-sensitive cardiac troponin T detection, Sens. Actuators B 308 (2020), https://doi.org/10.1016/J.SNB.2019.127630.
[68] Y.T. Lin, L.K. Wang, Y.T. Cheng, C.K. Lee, H.E. Tsai, Molecularly imprinted polymer/anodic aluminum oxide nanocomposite sensing electrode for low-concentration troponin T detection for patient monitoring applications, ACS Sens. 6 (2021) 2429–2435, https://doi.org/10.1021/acssensors.1c00738.